ORIGINAL PAPER

Structural, wide band gap half-metallic, and pressure-dependent thermodynamic predictions of Li_2TMMgO_6 (TM = V, Nb, and Ta) double perovskites

Wisam Ayad Ahmed Ahmed[1,2] · Evren Görkem Özdemir[1] · H. A. Rahnamaye Aliabad[3]

Abstract

Context Li_2VMgO_6, Li_2NbMgO_6, and Li_2TaMgO_6 double perovskite compounds were energetically the most stable in the FM phase. The lattice constants were 7.63 Å, 7.94 Å, and 7.95 Å, and the Curie temperatures were 910.451 K, 930.739 K, and 1258.821 K, respectively. The wide bandgap semiconductor characters were provided in the GGA-PBE methods as 2.139 eV, 4.209 eV, and 5.007 eV, respectively. This wide band gap semiconductor state in the majority carriers and the metallic state in the minority states made these double perovskites true half-metallic ferromagnetics. The bulk modulus obtained in the ground state calculations and the values obtained from thermodynamic calculations were relatively close. Debye temperatures in the initial state conditions were 747 K, 685.13 K, and 587.77 K, respectively. The total magnetic moment values were calculated as 3.00 μ_B/f.u. The most significant contribution to this value came from oxygen atoms.

Methods The theoretical calculations of Li_2VMgO_6, Li_2NbMgO_6, and Li_2TaMgO_6 double perovskite alloys were performed using the WIEN2k program developed by Blaha et al. The electronic calculations were made with GGA-PBE, GGA+mBJ, and GGA+U approximations in the space number 225 and the Fm-3 m symmetry group. The thermodynamic calculations were performed using Gibbs2. In thermodynamic calculations, temperature increases were determined as 100 K and temperature values were increased from 0 to 1200 K.

Keywords Wide band gap · Pressure-dependent · Half-metallic · Ferromagnetic · Double perovskite · Thermodynamics

Introduction

Interest in half-metallic materials has increased considerably since de Groot obtained the NiMnSb alloy as half-metallic ferromagnetic [1]. Half-metallic materials can show different electronic properties in different spin orientations [2–9]. While one of the majority or down spin orientations shows a metallic character, the other shows a semiconductor character [10–15]. Thus, as in the formula in Eq. 1, half-metallic materials show 100% spin polarization around Fermi energy levels.

$$P = \frac{n_\uparrow - n_\downarrow}{n_\uparrow + n_\downarrow} \times 100 \tag{1}$$

These types of materials are called true half-metallic materials. If the spin state, which has a semiconductor character, cuts the Fermi energy level at low density, the spin polarization will decrease, as seen in Eq. 1. In this case, the materials can be called nearly half-metallic [16–20]. The basis of spintronic applications is using spin-oriented materials in nano-sized devices. Therefore, true half-metallic materials are remarkable for spintronic applications due to their nature and ability to avoid being subjected to different polarization processes. Many studies, including half-metallic material groups, are carried out with the help of DFT calculations [21–24].

It is possible to see double perovskite materials being used in various areas [25, 26]. In 2021, Liu et al. [27]

✉ Evren Görkem Özdemir
evrengorkemozdemir@gazi.edu.tr

1   Department of Physics, Faculty of Science, Gazi University, 06560 Teknikokullar, Ankara, Türkiye

2   Department of Physics, Graduate School of Natural and Applied Sciences, Gazi University, Teknikokullar 06560, Ankara, Türkiye

3   Department of Physics, Hakim Sabzevari University, Sabzevar, Iran

produced wide-bandgap perovskite solar cells. Using the two-stage sequential deposition method, Liu et al. created perovskite solar cells with an energy band gap of 1.63 eV and a power conversion efficiency (PCE) of 20.35%. In 2023, Sun et al. [28] determined the solar cell material characteristics of $Cs_2B'B''X_6$ (B′ = Li, Na, K; B″ = In, Bi; X = Cl, Br, I) double perovskites using first-principles methods. Their study showed that $Cs_2B'In_{0.75}Bi_{0.25}I_6$ (B′ = Li, Na and K) double perovskite materials have direct band gaps in the optimal band gap ranges of 0.9 eV and 1.6 eV. In 2024, the electrochemical performances and energy storage applications of Dy_2CoMnO_6, Ra_2LaNbO_6, and Ba_2XIrO_6 (X = Y, La, Sc) double perovskite alloys were studied by Muddelwar et al. [29], Bairwa et al. [30], and Zanib et al. [31], respectively. Dy_2CoMnO_6 double perovskite alloy was synthesized in the monoclinic and P_{21}/n space groups. Muddelwar et al. achieved 87% stability in 10,000 cycles with Dy_2CoMnO_6 material, showing that this material is an excellent alternative electrode for energy storage. Bairwa et al. examined the structural and electronic properties of Ra_2LaNbO_6 double perovskite alloy using different approximations and obtained an indirect band gap of 2.4 eV in its electronic properties. Zanib et al. received the direct band gaps of Ba_2XIrO_6 (X = Y, La, Sc) double perovskite alloys as 2.7 eV, 2.6 eV, and 2.5 eV, respectively, in the majority electron states. They calculated the magnetic moment values of all these materials as 2.00 μ_B/f.u. The most partial contribution came from the transition metal iridium. Additionally, studies on first principles methods of X_2MnUO_6 (X = Sr or Ba), Sr_2EuReO_6, and Sr_2GdReO_6 double perovskite materials were carried out by Berri [32–34]. X_2MnUO_6 (X = Sr or Ba) materials were obtained as half-metallic materials, and their total magnetic moment value is 5.00 μ_B. Sr_2EuReO_6 and Sr_2GdReO_6 double perovskite materials also have high magnetic moment values of 8.00 μ_B and 9.00 μ_B, respectively. The total band gap in the Sr_2GdReO_6 compound was obtained as 2.02 eV. This study's half-metallic band gap value obtained using the GGA and GGA + U methods is 1.82 eV.

Lithium-containing materials have a large place in the literature, theoretically and experimentally. The physical and hydrogen storage properties of $LiMnH_3$ perovskite material were investigated by Usman et al. [35] in 2024. $LiMnH_3$ was obtained as a ferromagnetic material, and its hydrogen storage capacity was 4.67 wt%, showing that it is beneficial in this field. Tang [36] examined the hydrogen storage characteristics of K_2LiScH_6 and K_2LiAlH_6 double perovskite alloys in 2024. As a result of hydrogen storage processes, they observed that the gravimetric storage capacities of these materials could be increased to 4.41% and 5.08% with lithium doping. Pakravesh and Izadyar [37] investigated using $LiBX_3$ perovskites (B = Ge, Sn, Pb, X = F, Cl, Br, I) in photovoltaic devices using different structures. They showed that energy band gaps decrease with increasing atomic radii.

As a result of the calculations, Pakravesh and Izadyar proved that I-based $LiBX_3$ perovskites are more suitable for photovoltaic solar cells. As can be seen from all the examples, both lithium-containing metals with low electrochemical potential and perovskite materials, frequently used in solar cells, have a wide place in the literature experimentally and theoretically. In light of this information, the main purpose of this study is to examine the electronic, magnetic, and thermodynamic properties of lithium-based Li_2TMMgO_6 (TM = V, Nb, and Ta) double perovskite materials as a good alternative material that can be used for spintronic applications. As a result of ground state calculations, the Curie temperatures were higher than the room temperature. The magnetic moment values were relatively high. These results show that Li_2TMMgO_6 (TM = V, Nb, and Ta) double perovskites have been obtained as a suitable material group for spintronic applications.

Calculation method

The first-principles calculations of Li_2VMgO_6, Li_2NbMgO_6, and Li_2TaMgO_6 double perovskite alloys were performed using the WIEN2k program developed by Blaha et al. [38, 39]. The exchange–correlation energy E_{xc} was calculated using the Perdew, Burke, and Ernzerhof (PBE) version of Generalized Gradient Approximation (GGA). In the PBE-GGA scheme, the local spin density approximation (LSDA) can be calculated efficiently using adding gradient terms of the electron density $\nabla\rho(r)$ to the exchange–correlation energy. The exchange–correlation energy E_{xc} is a function of the local electron spin densities $\rho(r)$, and their gradient is given in Eq. 2:

$$E_{xc}^{GGA}(\rho_\uparrow, \rho_\downarrow) = \int \varepsilon_{xc}(\rho_\uparrow(r), \rho_\downarrow(r), \nabla\rho_\uparrow(r), \nabla\rho_\downarrow(r))\rho(r)d^3r$$

(2)

where ε_{xc}, $\rho_\uparrow$, and $\rho\downarrow$ are the exchange–correlation energy and electron densities for spin-up and spin-down states, respectively [40, 41]. Electronic calculations have also been investigated using Hubbard interactions (GGA + U) [42–44]. Hubbard interactions were applied for U = 1 eV, 2 eV, 3 eV, and 4 eV.

First, double perovskite alloys were created with the space number 225 and the Fm-3 m symmetry group and given in Fig. 1. Here, Li, {V/Nb/Ta}, Mg, and O atoms were placed at 0.25/0.25/0.25; {0/0/0}; 0.50/0/0, and 0.251/0/0 atomic positions, respectively.

Then, self-consistent functions (SCF) operations for each structure were carried out by selecting the 1728 k-point in the first Brillouin zone. The spin cut-off energy value for the initial calculations was determined as—7 Ry. $K_{max}R_{mt}$ and G_{max} values were set to 8 and 13 (a.u.)$^{-1}$. The optimization
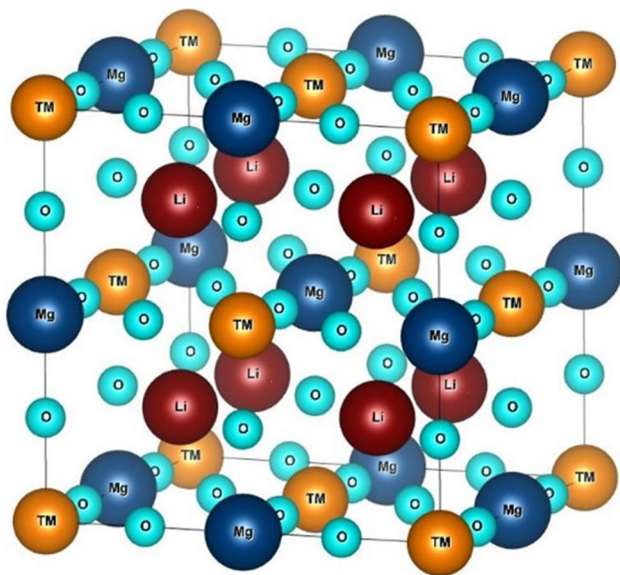
Fig. 1 The molecular structure of Li_2TMMgO_6 (TM = V, Nb, and Ta) double perovskite was created

processes were done by changing the equilibrium lattice point between -5% and 5% in 1% steps. Finally, the thermodynamic calculations were performed using Gibbs2 [45, 46]. Here, the pressure ranges were selected from 0 to 12 GPa in 1 GPa steps, and the temperature changes were determined from 0 to 1200 K in 100 K steps.

Results and discussion

The structural, electronic, half-metallic bandgap, and thermodynamic properties of Li_2VMgO_6, Li_2NbMgO_6, and Li_2TaMgO_6 double perovskites were investigated. First, the structural calculations were performed. The double perovskites were created in 225 space number and Fm-3 m symmetry group. To determine the ground state and magnetic phase values of double perovskite materials in this space

number and symmetry group, ferromagnetic (FM), antiferromagnetic (AFM), and non-magnetic (NM) phases were energetically optimized. While FM calculations were calculated by polarizing the spins of the materials, AFM calculations were obtained by aligning the spins of neighboring atoms up and down, respectively.

The FM phases of Li_2VMgO_6, Li_2NbMgO_6, and Li_2TaMgO_6 double perovskites were obtained as energetically the most stable phases. These obtained optimization curves are given in Fig. 2 for each double perovskite. The energy values in Fig. 2 were fitted with Murnaghan's equation of states (EOS) [47]. As a result of fitted curves, the obtained initial state values are given in Table 1. It is clear from the energy values in Fig. 2 and the data in Table 1 that the energy values of the FM phase are lower than those of the other phases. Lower energy means a more stable phase. Therefore, it can be said that each double perovskite in this study is a ferromagnetic material. According to the initial state values, the equilibrium lattice parameters of materials containing V, Nb, and Ta were obtained as 7.63 Å, 7.94 Å, and 7.95 Å, respectively. The increase in atomic radii as we move down the same period meets the expectations that these equilibrium lattice constants will also increase. There are also increases in volume values in proportion to the equilibrium lattice parameter.

In each material, the energy values of FM phases are lower than those of AFM phases. The energy differences between AFM and FM phases are 0.008661 Ry, 0.008854 Ry, and 0.011975 Ry for Li_2VMgO_6, Li_2NbMgO_6, and Li_2TaMgO_6 double perovskites, respectively. Theoretically, each double perovskite's Curie temperatures (T_c) can be determined using these energy differences and the formula below [48, 49].

$$T_C = \frac{2\Delta E_{AFM-FM}}{3k_\beta} \tag{3}$$

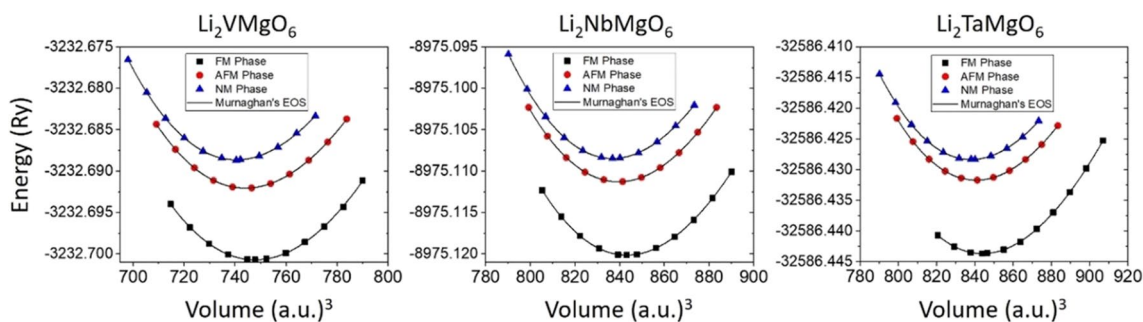Here, ΔE_{AFM-FM} is the energy difference between the AFM and FM phases and k_β is the Boltzmann's constant.

Fig. 2 The fitted FM, AFM, and NM volume-energy curves of Li_2VMgO_6, Li_2NbMgO_6, and Li_2TaMgO_6 double perovskites in 225 space number and Fm-3 m symmetry group

Table 1 The initial state values of Li_2VMgO_6, Li_2NbMgO_6, and Li_2TaMgO_6 double perovskites are in 225 space numbers and Fm-3 m symmetry group

Double Perovskite	Phases	a (Å)	B (GPa)	B'	V_0 (a.u.)^3	E_0 (Ry)	T_c (K)	E_{for} (eV)
Li_2VMgO_6	FM	7.63	126.85	2.99	747.849	-3232.70072	910.451	-49.782
	AFM	7.61	126.99	4.47	744.042	-3232.69206		
	NM	7.60	130.40	4.67	740.516	-3232.68863		
Li_2NbMgO_6	FM	7.94	124.86	4.39	843.170	-8975.12147	930.739	-51.449
	AFM	7.92	125.69	4.25	839.466	-8975.11129		
	NM	7.92	128.32	4.56	836.795	-8975.10847		
Li_2TaMgO_6	FM	7.95	129.92	4.23	843.918	32,586.44368	1258.821	-52.345
	AFM	7.93	131.61	4.45	840.738	32,586.43171		
	NM	7.92	133.35	4.83	838.040	32,586.42834		

With the help of Eq. 3, the Curie temperatures of Li_2VMgO_6, Li_2NbMgO_6, and Li_2TaMgO_6 double perovskites were obtained as 910.451 K, 930.739 K, and 1258.821 K, respectively. High Curie temperatures make these double perovskite materials excellent alternative materials for spintronic applications.

The formation energies of Li_2VMgO_6, Li_2NbMgO_6, and Li_2TaMgO_6 double perovskites were obtained with the help of Eq. 4.

$$E_{for} = E_{Li2TMMgO6} - \left(2 \times E_{Li}^{bulk} + E_{TM}^{bulk} + E_{Mg}^{bulk} + 6 \times E_O^{bulk} \right) \tag{4}$$

Energy values for Li, Mg, and O bulk materials were obtained as -15.04424 Ry, -400.66703 Ry, and -149.94118 Ry, respectively. The energy values of the transition metals V, Nb, and Ta bulk materials used in this study were calculated as -1898.63767 Ry, -7640.93583 Ry, and -31,252.19219 Ry, respectively. The total energy values obtained as a result of these bulk calculations were obtained as -3229.04026 Ry, -8971.33842 Ry, and -32,582.59478 Ry for Li_2VMgO_6, Li_2NbMgO_6, and Li_2TaMgO_6 double perovskites, respectively. As a result, the formation energy values of each double perovskite material were obtained with the help of Eq. 4, which is given in Table 1. The negative formation energy values indicate the structural stability of each double perovskite in this study.

Figures 3 and 4 show the band structures and total densities of states (TDOS) for both majority and minority spin states of (a) Li_2VMgO_6, (b) Li_2NbMgO_6, and (c) Li_2TaMgO_6 double perovskite materials obtained for GGA and GGA + mBJ approximations. In these figures, horizontal dotted lines indicate Fermi energy levels. In Fig. 3, the minority electrons cross the Fermi energy levels for each double perovskite.

The valence electrons can move to conduction bands. Therefore, minority electron states show metallic character for each double perovskite. In Li_2VMgO_6 double perovskite, there is a gap between 1 eV and 1.5 eV between the valence band maximum electrons passing into the conduction band and the conduction band minimum electron densities. Although the metallic character continues for the elements in the same group, the band gap values between the maximum values of the valence electrons passing into the conduction band and the minimum values of the conduction band electrons increase interestingly. Therefore, the results obtained using the GGA-PBE approximation suggest that although the minority electron states show metallic character, there may also be situations where semiconductor characters may emerge. In majority electron densities, it is possible to see apparent band gaps between the valence band values and conduction band values for each double perovskite. Therefore, the majority electron states show semiconductor character. It is seen in Fig. 3 that the band gap values increase when Ta, Nb, and V elements are used. This situation is the same as that encountered in minority electron states. However, in the majority electron states, semiconductor characters emerged instead of metallic characters. VBM and CBM minimum values are at Γ-points. The band gap values for Li_2VMgO_6, Li_2NbMgO_6, and Li_2TaMgO_6 double perovskites are 2.139 eV, 4.209 eV, and 5.007 eV, respectively. All these obtained values are given in Table 2. Therefore, the majority electron states of Li_2VMgO_6, Li_2NbMgO_6, and Li_2TaMgO_6 double perovskites have a semiconductor nature with direct wide band gaps. As seen in Table 2, VBM and CBM values increase according to changing transition metals. The values closest to the Fermi energy level values are the VBM values. Therefore, the half-metallic band gap values of Li_2VMgO_6, Li_2NbMgO_6, and Li_2TaMgO_6 double perovskites were obtained as 0.235 eV, 0.240 eV, and 0.250 eV, respectively. As a result, each double perovskite material in this study is a true half-metallic ferromagnetic material that combines metallic and semiconductor characteristics.

Figure 4 shows the band structures and total densities of states of Li_2VMgO_6, Li_2NbMgO_6, and Li_2TaMgO_6 double perovskites obtained using the GGA + mBJ approximation. Compared to GGA-PBE calculations, in this method, the electronic properties of the minority
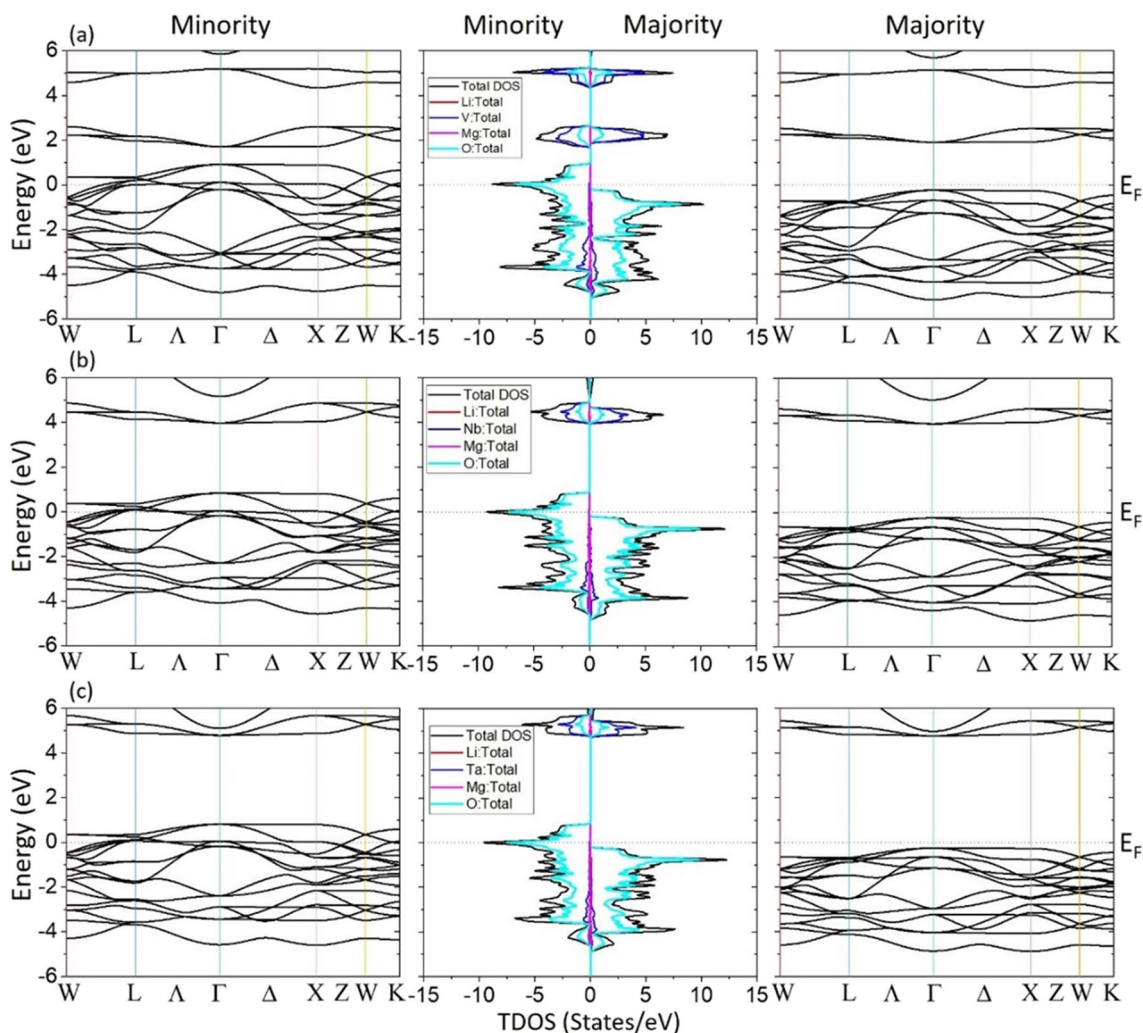
Fig. 3 The plotted band structures and total densities of states (TDOS) of (**a**) Li_2VMgO_6, (**b**) Li_2NbMgO_6, and (**c**) Li_2TaMgO_6 double perovskites in 225 space number (Fm-3 m symmetry group) for GGA-PBE approximation

electrons show a metallic character. In the majority electron state, each double perovskite shows a semiconductor character. When the GGA + mBJ approximation is used, the band gaps are significantly increased. While the band gap of Li_2VMgO_6 double perovskite is 4.362 eV, the band gaps of Li_2NbMgO_6 and Li_2TaMgO_6 double perovskites are 6.042 eV and 7.319 eV, respectively, and these two materials have begun to exhibit insulating characters in the majority electron states. VBM and CBM values and total band gap values for each double perovskite are given in Table 2. According to Table 2, VBM and CBM values increased significantly compared to the GGA + PBE approximation.

The energy gaps closest to the Fermi energy level were calculated as 2.126 eV, 1.872 eV, and 1.823 eV for Li_2VMgO_6, Li_2NbMgO_6, and Li_2TaMgO_6 double perovskites, respectively. According to the GGA + mBJ

approximation, the half-metallic band gaps of each double perovskite increased sharply.

The partial densities of states (PDOS) of Li_2VMgO_6, Li_2NbMgO_6, and Li_2TaMgO_6 double perovskites are given in Fig. 5 to examine which atomic and orbital states the electron densities coming to the band structures come from. In Figs. 3 and 4, the most significant contribution to TDOS comes from the oxygen (cyan color) atom. This is also true for each double perovskite in this study. The main contributions from the majority electron carriers of Li, Mg, and O atoms are from p-orbitals. This is an expected value. The densities of each major partial state are shown as dashed lines. Partial electron densities from the transition metals V, Nb, and Ta are in the d-orbitals. These results also meet expectations. When the electron density states around the Fermi energy levels are examined, the s and p orbitals of Li atoms also cut the Fermi energy levels in the minority
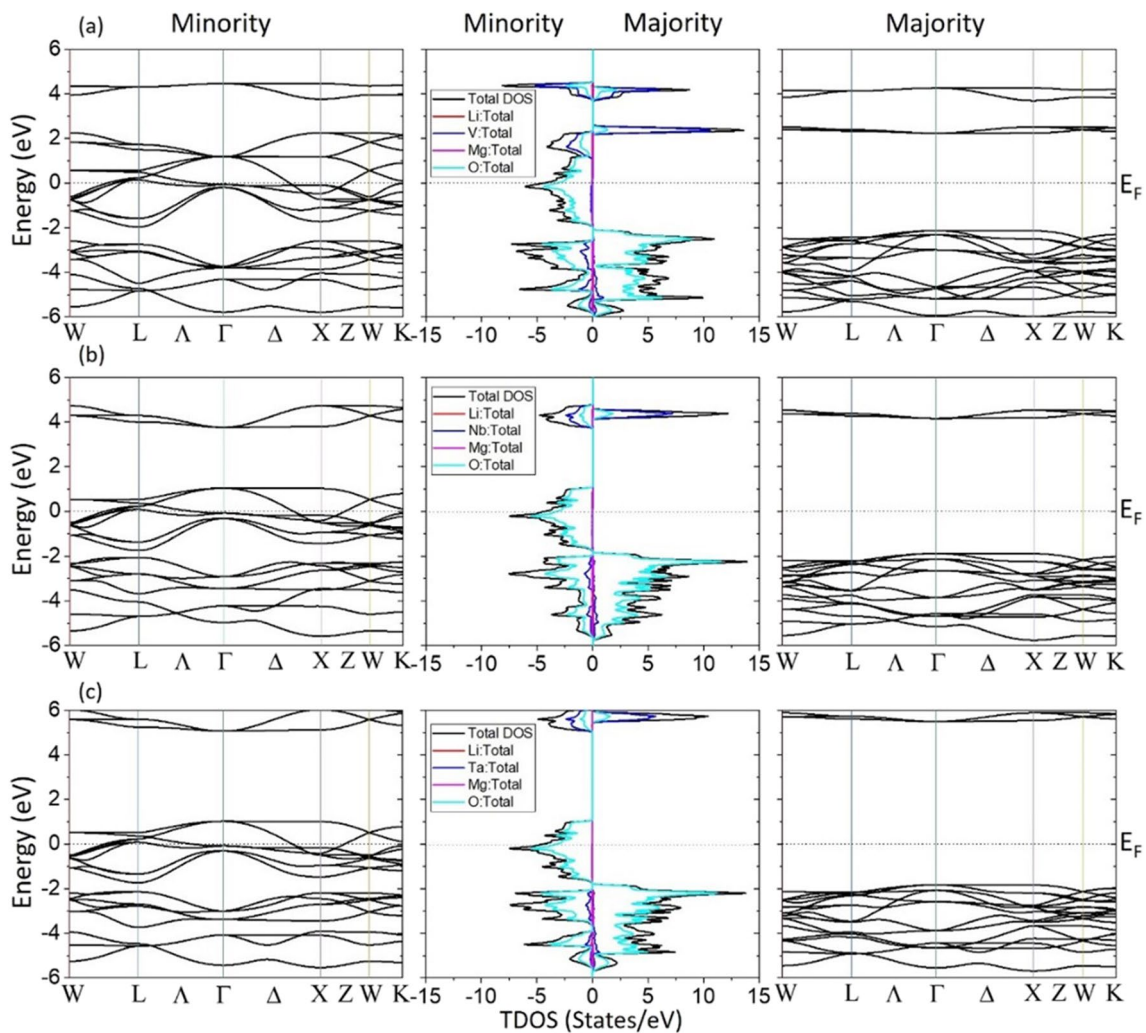
Fig. 4 The plotted band structures and total densities of states (TDOS) of (**a**) Li_2VMgO_6, (**b**) Li_2NbMgO_6, and (**c**) Li_2TaMgO_6 double perovskites in 225 space number (*Fm-3 m* symmetry group) for GGA + mBJ approximation

Table 2 The calculated VBM, CBM, and band gaps of Li_2VMgO_6, Li_2NbMgO_6, and Li_2TaMgO_6 double perovskites for 225 number

Double Perovskite (*Fm-3 m, 225*)	$VBM^{Majority}$ (eV) GGA-PBE	$CBM^{Majority}$ (eV) GGA-PBE	$Gap^{Majority}$ (eV) GGA-PBE	$VBM^{Majority}$ (eV) GGA + mBJ	$CBM^{Majority}$ (eV) GGA + mBJ	$Gap^{Majority}$ (eV) GGA + mBJ
Li_2VMgO_6	-0.235	1.904	2.139	-2.126	2.236	4.362
Li_2NbMgO_6	-0.240	3.969	4.209	-1.872	4.170	6.042
Li_2TaMgO_6	-0.250	4.757	5.007	-1.823	5.496	7.319

electron states. However, the contributions from the p orbital are much higher than those from the s orbital. In the majority of electron states, the semiconductor character arises from the density differences between the p-orbitals of the Li atom.

Most partial contributions to the total density of states come from the oxygen atom. The p-orbitals of the oxygen atom provide the semiconductor characteristics in the majority band states, and the sharp peak in the minority electron

states that cut the Fermi energy level. The contributions of transition metals V, Nb, and Ta atoms around the Fermi energy levels are quite low. Distributions from d-orbitals, the majority electron carriers of these transition metals, are concentrated in distant energy regions. Mainly, the atoms that cause the minority electron states to show metallic character by cutting the Fermi energy levels are Li, Mg, and O. Although the sharp peaks of the partial electron densities of
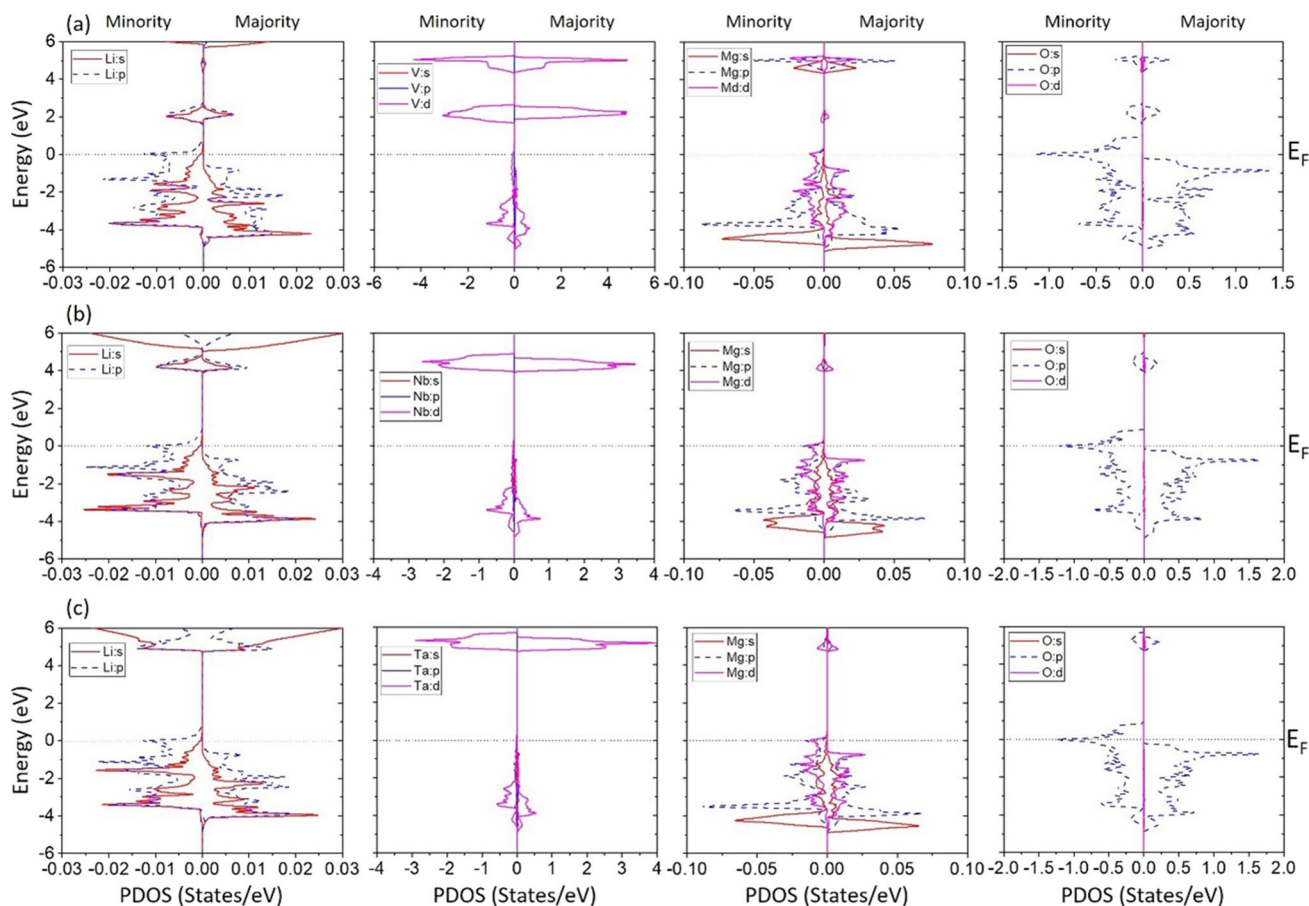
Fig. 5 The obtained partial densities of states (PDOS) of (**a**) Li_2VMgO_6, (**b**) Li_2NbMgO_6, and (**c**) Li_2TaMgO_6 double perovskites

the Li and Mg atoms are far from the Fermi energy levels, in minority cases these peaks are concentrated exactly above the Fermi energy levels. However, all the sharp peaks from the O atom are in energy regions very close to the Fermi energy levels. In most electron states, the valence band is between 0 eV and -1 eV, which shows semiconductor character. These contributions are quite small in the conduction band of the majority electron states. In the minority electron states, sharp electron folds from the O atom, and its p-orbitals are visible. There is a sharp intensity increase towards the maximum values of the valence band; the intensity peak reaches its maximum value above the Fermi energy level and begins to decrease in the 0 eV to 1 eV range of the conduction band. Therefore, oxygen is the atom that sharply distinguishes the electronic properties of the alloys obtained in this study.

In Fig. 6, the band gap changes in the Fm-3 m symmetry group of Li_2TMMgO_6 (TM = V, Nb, and Ta) double perovskites are given as a function of V/V_0. The values in Fig. 6 and Table 2 support Figs. 3 and 4. As can be seen, as the atomic radii of atoms in the same group increase, the energy band gaps also increase. Since only selected V, Nb, and Ta
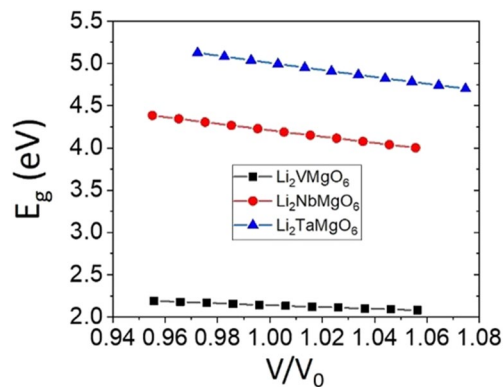

Fig. 6 The calculated band gap values of Li_2VMgO_6, Li_2NbMgO_6, and Li_2TaMgO_6 double perovskites as a function of V/V_0

transition metals were changed in the ground state values when creating Li_2VMgO_6, Li_2NbMgO_6, and Li_2TaMgO_6 double perovskites, these sharp increases in band gaps can be thought to be due to the increasing atomic radius. This is the main reason for the increases in band gap values. The minority electron states of each material have a metallic

character. Increasing atomic radii did not cause any effect in minority electron states.

In the majority electron states, the increase in atomic radius sharply changed the energy amounts between VBM and CBM. As seen in Table 2, VBM values are almost the same for double perovskites containing V, Nb, and Ta. However, the CBM values increased remarkably with the increase in atomic radii. The electron densities at CBM values belong to O (cyan) and the transition metals V, Nb, and Ta (blue). Although the density of the O atom is much less than that of V, Nb, and Ta transition metals, the initial and final energy values of the electron densities are the same. Therefore, increasing atomic radii increases the electron density interaction energy values between O and V, Nb, and Ta.

In addition to GGA-PBE and GGA + mBJ approximations, Hubbard interactions of Li_2TMMgO_6 (TM = V, Nb, and Ta) double perovskites were also examined to compare electronic calculations. Hubbard interaction parameters were determined as U = 1 eV, 2 eV, 3 eV, and 4 eV. The band structures of the electronic properties obtained with each interaction are given in Figs. 7, 8 and 9 for Li_2VMgO_6, Li_2NbMgO_6, and Li_2TaMgO_6 double perovskites, respectively.

When Hubbard interactions are applied to Li_2TMMgO_6 (TM = V, NB, Ta) double perovskites, they change the band structures. It shows properties similar to those of GGA-PBE and GGA + mBJ approximations in majority and minority band structures. While the minority band structures show metallic characters, the majority band structures have semiconductor characters. As the Hubbard potential is applied to Li_2VMgO_6 and Li_2NbMgO_6 double perovskites

increases, the energy gaps in the majority band states are observed. In GGA-PBE approximation, the band gap values of Li_2VMgO_6 and Li_2NbMgO_6 double perovskites are 2.139 eV and 4.209 eV, respectively, while at U = 1 eV, these values are calculated as 2.242 eV and 4.305 eV, respectively.

A slight increase in the band gap of both materials was observed due to the Hubbard interaction. However, as the amount of U increases, the increases in the energy band gaps are clearer. For U = 4 eV, the band gaps of Li_2VMgO_6 and Li_2NbMgO_6 double perovskites are 2.574 eV and 4.601 eV, respectively. All these values are given in Table 3. The main reason for these changes in band gap values is the increase in the conduction band minimum values. As a result of the Hubbard interactions applied at the valence band maximum values, the changes are almost zero. However, when the conduction band minimum values are examined, it can be said that Hubbard interactions directly affect the conduction band values.

When 1 eV and 2 eV Hubbard interactions are applied to Li_2TaMgO_6 double perovskite, the energy bandwidth in the majority band states increases. These increases decrease at 3 eV and 4 eV values. In all cases, the resulting band gap values are more significant than the GGA-PBE values. While VBM values remained constant in Li_2TaMgO_6 double perovskite, energy band changes were also seen in CBM values. While the closest electrons in the valence band around Fermi energy levels belong to oxygen atoms (shown in cyan color in the TDOS), the electron densities in the conduction band belong to V, Nb, and Ta atoms (shown in blue color in the TDOS). Therefore, the electron densities that determine the band gaps are the electron densities of oxygen atoms in the valence band and the electron densities of V, Nb, and Ta
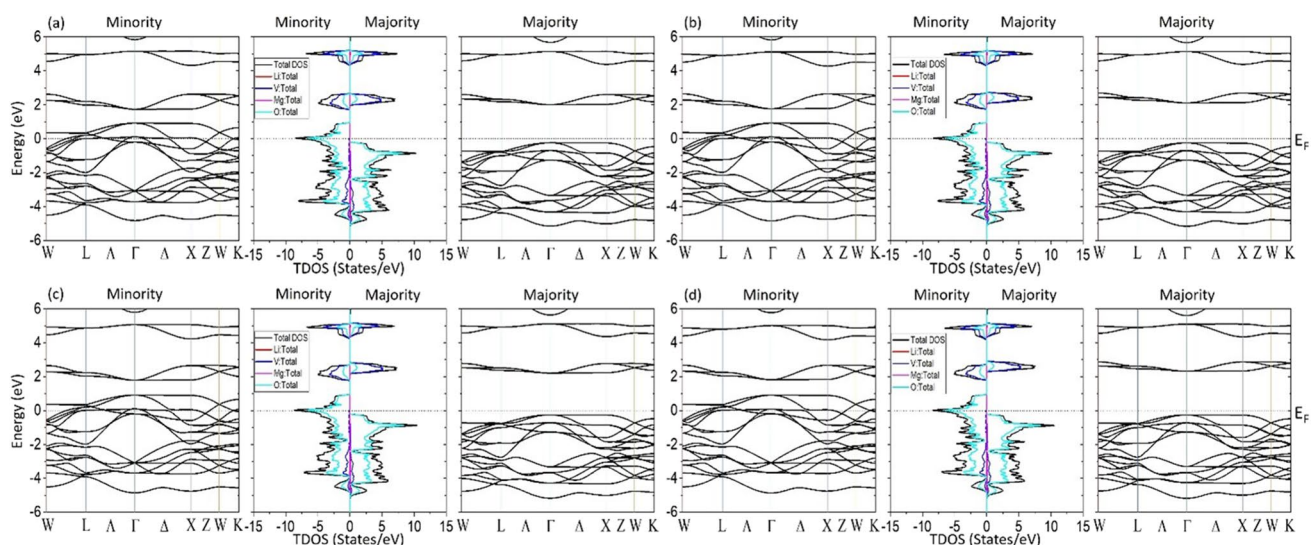

Fig. 7 The plotted band structures and total densities of states (TDOS) of Li_2VMgO_6 double perovskite for GGA + U **a**) U = 1 eV, **b**) U = 2 eV, **c**) U = 3 eV, and **d**) U = 4 eV
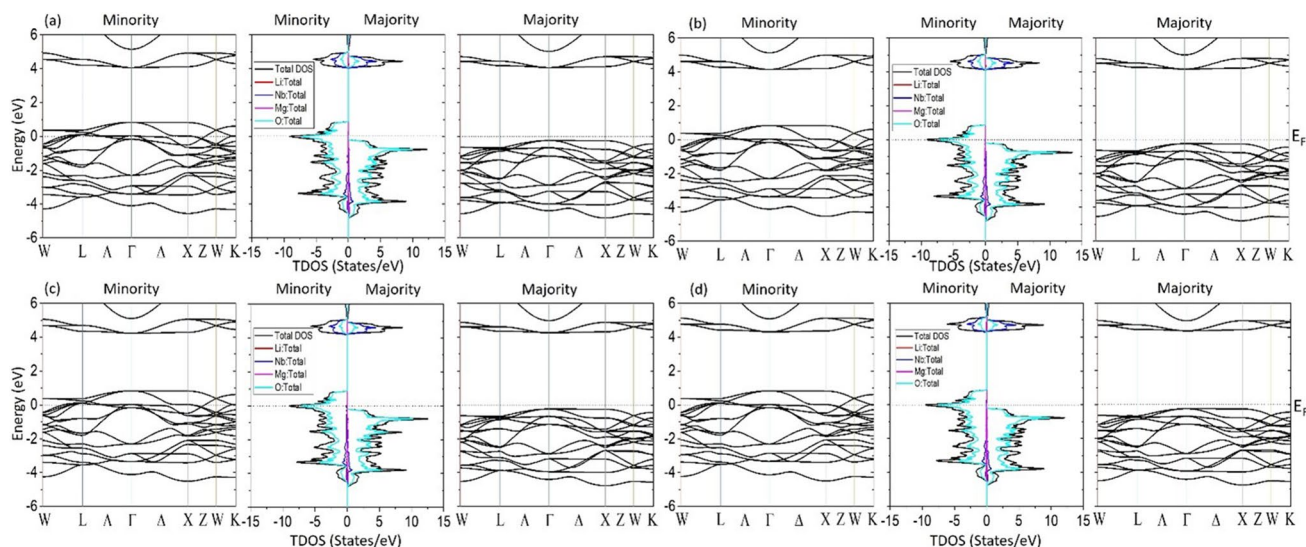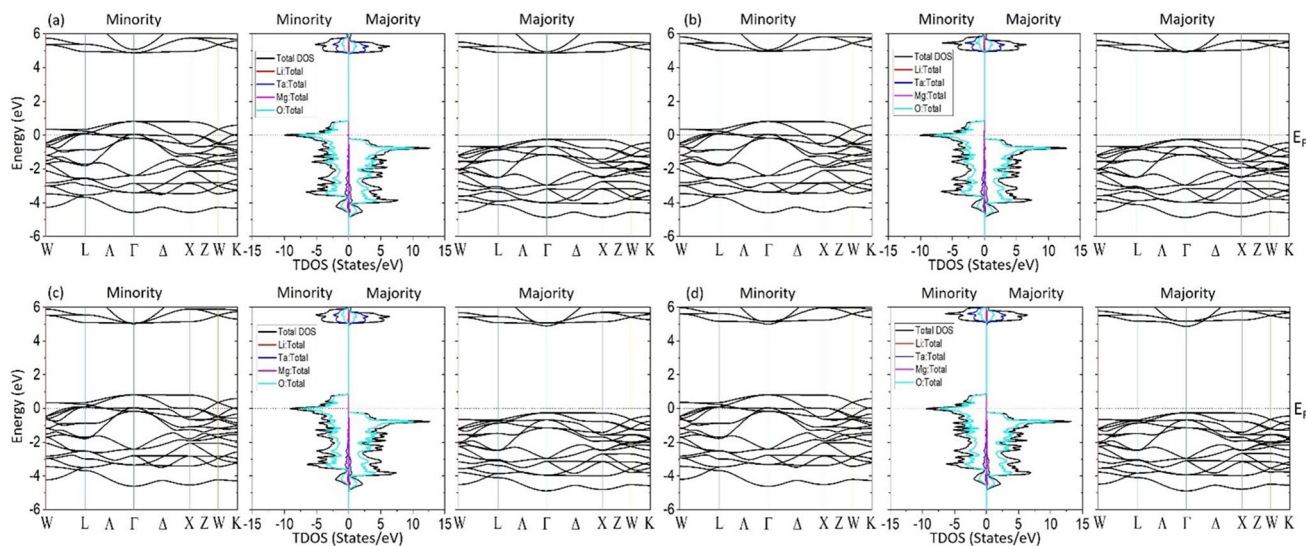
Fig. 8 The plotted band structures and total densities of states (TDOS) of Li_2NbMgO_6 double perovskite for GGA + U **a**) U = 1 eV, **b**) U = 2 eV, **c**) U = 3 eV, and **d**) U = 4 eV

Fig. 9 The plotted band structures and total densities of states (TDOS) of Li_2TaMgO_6 double perovskite for GGA + U **a**) U = 1 eV, **b**) U = 2 eV, **c**) U = 3 eV, and **d**) U = 4 eV

atoms, which are transition metals in the conduction bands. As a result, the constant valence band maximum values and changes in conduction band minimum values indicate that Hubbard interactions are effective on V, Nb, and Ta transition metals.

Thermodynamic properties of Li_2VMgO_6, Li_2NbMgO_6, and Li_2TaMgO_6 double perovskites, such as bulk moduli, Debye temperature, entropy, heat capacity, vibrational, and vibrational-free energy values, depending on pressure and temperature, were examined using the Gibbs2 software [45, 46]. Bulk modulus values depending on pressure and temperature are given in Fig. 10. While the bulk modulus values increase as the pressure increases, they decrease as the temperature increases. The bulk modulus values of Li_2VMgO_6, Li_2NbMgO_6, and Li_2TaMgO_6 double perovskites at 0 GPa pressure and 0 K temperature were obtained as 120.4751 GPa, 117.9561 GPA, and 123.3624 GPa, respectively. Under 12 GPa, the maximum pressure applied for thermodynamic calculations, these values were obtained as 169.5216 GPa, 168.8855 GPa, and 180.3451 GPa, respectively.

Table 3 The calculated VBM, CBM, and band gaps of Li_2VMgO_6, Li_2NbMgO_6, and Li_2TaMgO_6 double perovskites for using Hubbard interactions

Double Perovskite (*Fm-3 m, 225*)	U (eV)	VBM^{Majority} (eV)	CBM^{Majority} (eV)	Gap^{Majority} (eV)
Li_2VMgO_6	1	-0.239	2.003	2.242
	2	-0.243	2.107	2.350
	3	-0.248	2.210	2.458
	4	-0.254	2.320	2.574
Li_2NbMgO_6	1	-0.241	4.064	4.305
	2	-0.241	4.162	4.403
	3	-0.241	4.260	4.501
	4	-0.241	4.360	4.601
Li_2TaMgO_6	1	-0.250	4.860	5.110
	2	-0.250	4.918	5.168
	3	-0.250	4.893	5.143
	4	-0.250	4.868	5.118

As can be seen, the reactions to an increase in external pressure are different. While the bulk modulus difference between Li_2VMgO_6 and Li_2NbMgO_6 was approximately 2.5 GPa at 0 GPa external pressure, this difference decreased to about 0.7 GPa under 12 GPa external pressure. In Li_2TaMgO_6 double perovskite, increasing external pressure directly increased the bulk modulus of this alloy.

Therefore, the resistance to volume change is highest in Li_2TaMgO_6 double perovskite. Additionally, bulk modulus values obtained from base case calculations are also given in Table 1. According to these results, the bulk moduli of Li_2VMgO_6, Li_2NbMgO_6, and Li_2TaMgO_6 double perovskite alloys were calculated as 126.85 GPa, 124.86 GPa, and 129.92 GPa, respectively. The values obtained from both the ground state values and thermodynamic calculations are very close to each other. Figure 11 shows the Debye temperature values of double perovskite alloys depending on pressure and temperature. Debye temperatures at 0 GPa pressure and 0 K temperature were calculated as 747 K, 685.13 K, and 587.77 K for Li_2VMgO_6, Li_2NbMgO_6, and Li_2TaMgO_6 double perovskites, respectively. As the temperature increases, the Debye temperature decreases, and as the pressure rises, the Debye temperature increases. This is true for each alloy. Compared to the different transition metals in the same group used in this study, there is a sharp decrease in Debye temperatures as atomic radii increase.

Figure 12 shows the changes in entropy and specific heat capacities (C_v and C_p) depending on pressure and temperature. It is possible to see an almost linear line between 0–100 K temperature in entropy values. However, starting from 100 K, entropy parameters increase with the increase in temperature. Unlike other calculated parameters, specific heat capacities and entropy values decrease with increasing pressure. These parameters have zero values at 0 K
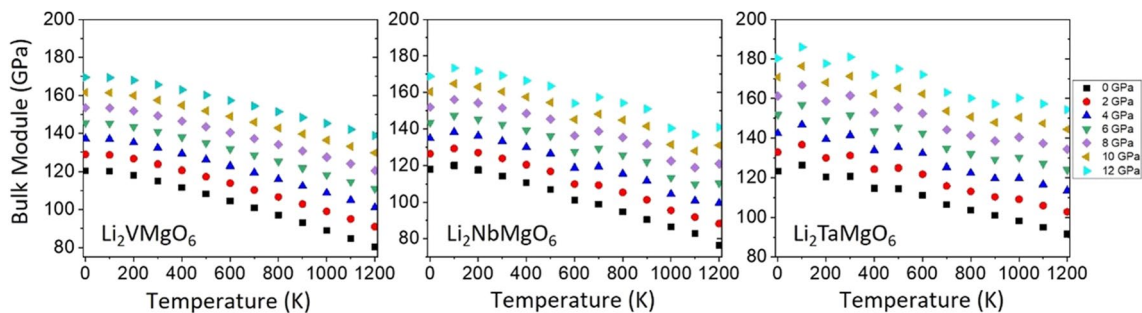
Fig. 10 The calculated pressure–temperature-dependent bulk moduli of Li_2VMgO_6, Li_2NbMgO_6, and Li_2TaMgO_6 double perovskites
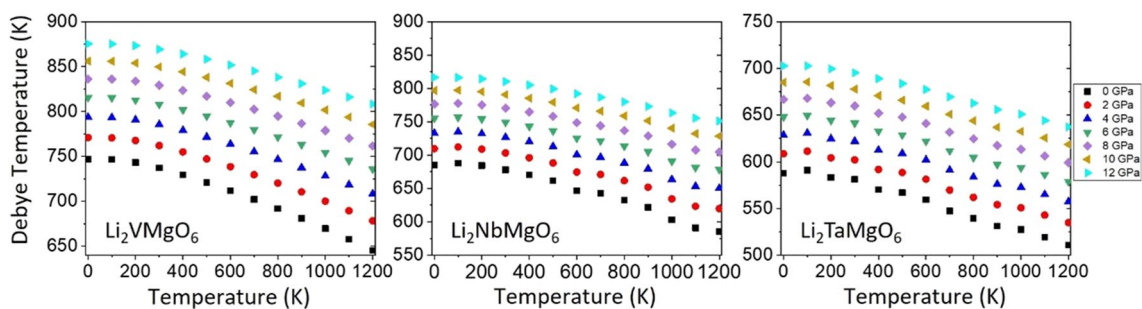
Fig. 11 The calculated pressure–temperature-dependent Debye temperatures of Li_2VMgO_6, Li_2NbMgO_6, and Li_2TaMgO_6 double perovskites

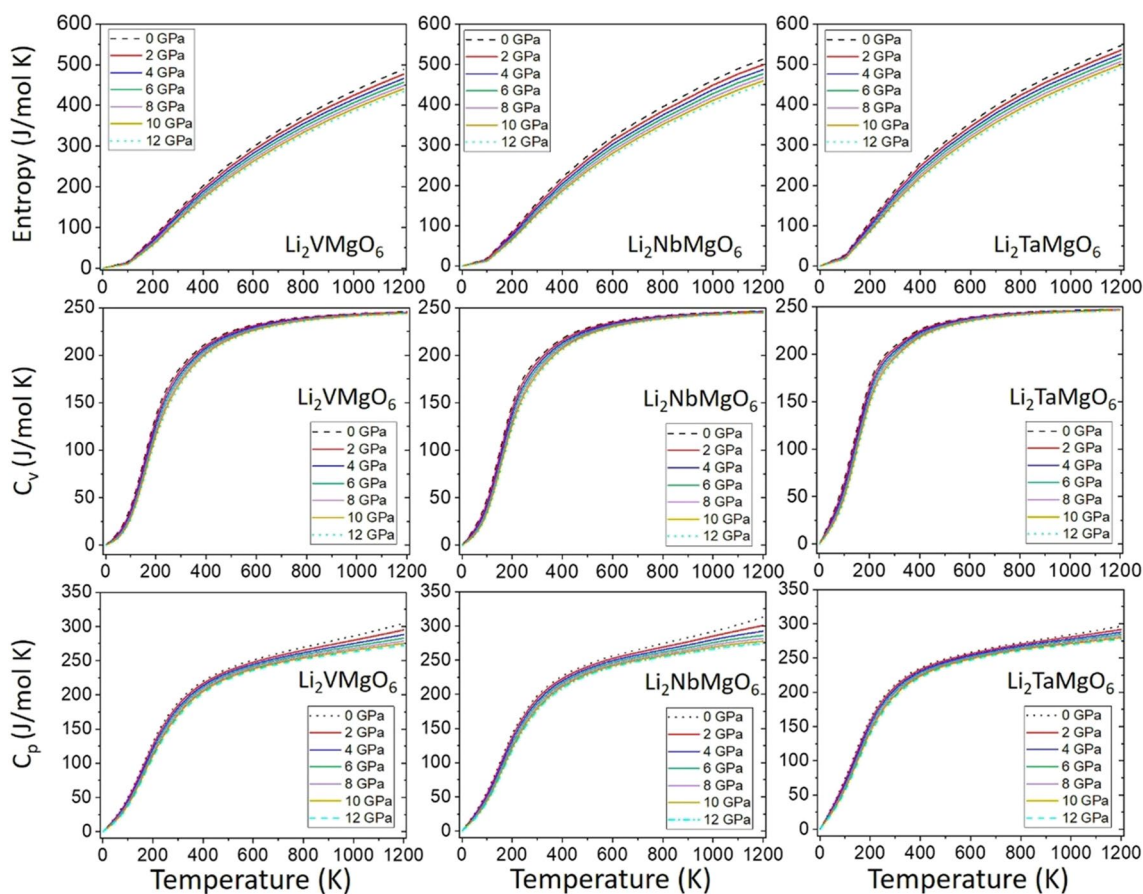**Fig. 12** The calculated pressure–temperature-dependent entropy and heat capacity variations of Li_2VMgO_6, Li_2NbMgO_6, and Li_2TaMgO_6 double perovskites

and 0 GPa pressure. At 100 K temperature, the entropy values of Li_2VMgO_6, Li_2NbMgO_6, and Li_2TaMgO_6 double perovskites are 14.84006 J/mol K, 18.52276 J/mol K, and 27.45239 J/mol K. As can be seen, as the atomic radius increases, entropy values also increase. At 0 GPa and 200 K temperature, these values are 74.66984 J/mol K, 86.39708 J/mol K, and 111.8111 J/mol K. A sharp increase in entropy changes with the temperature rise is seen. When the temperature increases to 1200 K, the highest temperature used in these calculations, the entropy values become 489.1478 J/mol K, 513.0991 J/mol K, and 546.7725 J/mol K. It can be said that C_v and C_p values are compatible with the Dulong–Petit law [50] in the temperature range of 0–300 K. After 300 K, the increase amounts decrease considerably. While the C_v of Li_2VMgO_6 double perovskite alloy is constant starting from 1000 K temperature, the C_v of Li_2NbMgO_6 and Li_2TaMgO_6 double perovskite alloys are almost constant starting from 800 K temperature.

The C_v values at 0 GPa pressure and 300 K temperature are 187.7838 J/mol K, 195.7365 J/mol K, and 208.2529 J/mol K. The C_v of Li_2VMgO_6 double perovskite alloy at 1000 K temperature is 243.9298 J/mol K, while the C_v of

Li_2NbMgO_6 and Li_2TaMgO_6 double perovskite alloys at 800 K temperature are 241.8072 J/mol K and 243.858 J/mol K, respectively. Although there are differences between the C_v of each double perovskite alloy, these values are very close. In other words, changing atomic radii did not cause much change in the C_v.

Total and partial magnetic moment values of Li_2VMgO_6, Li_2NbMgO_6, and Li_2TaMgO_6, double perovskite alloys, were calculated. The total magnetic moment of each alloy was obtained as 3.00 μ_B/f.u. This is the expected value since the changing elements in these alloys are transition metals in the same group. In these three alloys, the partial contributions from lithium atoms are -0.00687 μ_B, -0.00801 μ_B, and -0.00836 μ_B, respectively, while the partial contributions from magnesium atoms are -0.00339 μ_B, -0.0050 μ_B, and -0.00493 μ_B, respectively. The partial contributions from transition metals V, Nb, and Ta atoms are -0.28577 μ_B, -0.10357 μ_B, and -0.08119 μ_B, respectively. The partial magnetic moment contributions of lithium and magnesium atoms are quite low. In the contributions from transition metals, it has been observed that the magnetic contribution decreases as the group number increases. The main contributions from

oxygen atoms in each double perovskite alloy are 0.50039 μ_B, 0.48185 μ_B, and 0.47157 μ_B, respectively. As can be seen, the main magnetic carriers in Li_2TMMgO_6 (TM = V, Nb, and Ta) double perovskite alloys are oxygen atoms.

Conclusion

Electronic, structural, half-metallic, magnetic, and thermodynamic properties of Li_2VMgO_6, Li_2NbMgO_6, and Li_2TaMgO_6 double perovskite alloys were investigated using WIEN2k program. In Li_2VMgO_6, Li_2NbMgO_6, and Li_2TaMgO_6 double perovskite alloys, the lowest energy values were obtained in the FM phases. The lattice parameters were obtained at the lowest energy values as 7.63 Å, 7.94 Å, and 7.95 Å, respectively. The Curie temperatures were calculated as 910.451 K, 930.739 K, and 1258.821 K for Li_2VMgO_6, Li_2NbMgO_6, and Li_2TaMgO_6. Their high Curie temperatures make these materials very attractive for spintronics applications. According to the electronic properties of each alloy, the minority spin states have a metallic character. In contrast, the majority spin states have a semiconductor nature. In GGA-PBE approximation, semiconductor band gaps were calculated as 2.139 eV, 4.209 eV, and 5.007 eV for Li_2VMgO_6, Li_2NbMgO_6, and Li_2TaMgO_6 alloys, respectively. In transition metals, the band gap widens as the atomic radii increase. In all three alloys, the valence band values are closer to the Fermi energy levels. Therefore, the valence band values determine the half-metallic band gap values. The half-metallic band gaps are 0.235 eV, 0.240 eV, and 0.250 eV, respectively. In GGA + U (U = 1 eV, 2 eV, 3 eV, and 4 eV), the energy band gaps obtained from each applied Hubbard interaction are larger than those obtained with GGA-PBE. These increases affect the transition metals in the conduction band, increasing the electron density values of the transition metals. When the GGA + mBJ approximation was used, the obtained band gap values increased so much that Li_2VMgO_6 (4.362 eV), Li_2NbMgO_6 (6.042 eV), and Li_2TaMgO_6 (7.319 eV) double perovskites started to show insulating characters in this approximation. The bulk modulus values obtained in thermodynamic and ground state calculations are almost the same. Debye temperatures of Li_2VMgO_6, Li_2NbMgO_6, and Li_2TaMgO_6 double perovskites were obtained as 747 K, 685.13 K, and 587.77 K at 0 GPa and 0 K temperature. It has been observed that the Debye temperature decreases as the period changes in different transition metals. At the same time, the total magnetic moment was obtained as 3.00 μ_B/f.u. for each material. The oxygen atom was the most significant contribution to the total magnetic moment. Oxygen atoms play the main role in the carrier of these materials.

Declarations

References

1. de Groot RA, Mueller FM, van Engen PG, Buschow KHJ (1983) New class of materials: half-metallic ferromagnets. Phys Rev Let 50:2024. https://doi.org/10.1103/PhysRevLett.50.2024

2. Monir MA, Baltach H, Al-Maaitah IF, A-MaaitahGhebouliFatmiAlbawamiMohammadDebbichiSillanpaa AFMAMMDSMM (2024) Half-metallic ferromagnetic features of V-doped Cu_2O alloys: TB-mBJ and DFT + U insights. Res Phys 57:107368. https://doi.org/10.1016/j.rinp.2024.107368

3. Özdemir EG, Merdan Z (2020) Comparisons of half-metallic results of $Al_{0.75}Co_{0.25}Sb$ diluted magnetic semiconductor with generalized gradient approximation (GGA) and Tran Blaha modified Becke-Johnson (TB_mBJ) potential methods. Physica B 581:411841. https://doi.org/10.1016/j.physb.2019.411841

4. Monir MEA, Baltach H, Al-Maaitah IF, A-MaaitahLaref AFA (2024) First-principles study of structural, electronic and optoelectronic properties of Ag-doped Cu_2O alloys: TB-mBJ insights. Modern Phys Lett B 38:2450036. https://doi.org/10.1142/S0217984924500362

5. Laghzaoui L, Lamrani AF, Ahl Laamara R (2023) Robust half-metallic ferromagnet in doped double perovskite Sr_2TiCoO_6 by rare-earth elements for photovoltaic and thermoelectric conversion: A DFT method. J Phys Chem Sol 188:11639. https://doi.org/10.1016/j.jpcs.2023.111639

6. Laghzaoui S, Lamrani AF, Ahl Laamara R (2023) Excellent optical and thermoelectric features of two-dimensional half-metallic ferromagnet $Zn_{1-x}(TM)_xO$: A first principle investigation. Physica B 668:415241. https://doi.org/10.1016/j.physb.2023.415241

7. Peng K, Zhang M, Zhang C, Ma L, Liu Y, Zhao J, Wang R (2024) A DFT study on half-metallicity of Ruddlesden-Popper layered perovskite $Bi_8Ba_4Mn_8O_{28}$. Physica B 674:415587. https://doi.org/10.1016/j.physb.2023.415587

8. Özdemir EG (2022) Effects of atomic displacements on band gaps of Na_2MgXO_6 (X= Co, Fe) double perovskite oxides: GGA and GGA+U approaches. Mat Sci Semicond Proc 152:107078. https://doi.org/10.1016/j.mssp.2022.107078

9. Özdemir EG (2022) The half-metallic predictions of M (M = Y, Zr, Nb)–Sc–Sn diluted ternary alloys via GGA and GGA + mBJ. Eur Phys J B 95:129. https://doi.org/10.1140/epjb/s10051-022-00388-9

10. Ati AH, Kadhim AA, Abdulhussain AA, Abed WA, Kadhim KF, Nattiq MA, Al-zyadi JMK (2024) Computational study of half-metallic behavior, optoelectronic and thermoelectric properties of new $XAlN_3$ (X = K, Rb, Cs) perovskite materials. J Phys Chem Sol 188:111899. https://doi.org/10.1016/j.jpcs.2024.111899

11. Wang LY, Hu LL, Huang CC, Wang Y, Liu J (2024) First-principles study on a promising intrinsic d^0f^0-type half-metallic nanosheet LaS_2 with high Curie temperature. Mat Sci Eng B 299:116957. https://doi.org/10.1016/j.mseb.2023.116957

12. Chinnadurai K, Natesan B (2024) Influence of main-group elements on structural, electronic, magnetic and half-metallic properties of DO_3-type Mn_3Z (Z = Al, Ga, In, Si, Ge, Sn, P, As and Sb) alloys - A DFT study. Comp Cond Mat 38:e00871. https://doi.org/10.1016/j.cocom.2023.e00871

13. Özdemir EG, Doğruer S, Özcan A, Merdan Z (2022) The effect of structural changes on half-metallic, elastic and magnetic properties of the FeWGa half-Heusler compound via first-principles studies. J Magn Magn Mat 546:168872. https://doi.org/10.1016/j.jmmm.2021.168872

14. Özdemir EG, Doğruer S (2023) The structural, magnetic, and pressure-induced elastic predictions of $ZrPd_2O_4$ oxide spinel via GGA, GGA+mBJ, and GGA+U approximations. J Magn Mag Mat 568:170417. https://doi.org/10.1016/j.jmmm.2023.170417

15. Elkenany EB, Othman MS (2021) Influence of pressure and temperature on mechanical and thermal behaviors of InAsSb and GaAsSb alloys. Phy Scripta 96:125718. https://doi.org/10.1088/1402-4896/ac3270

16. Nazir S, Liaqat T, Alvi K, Zulfiqar M (2023) Biaxial ([110]) strain influence on the n-type half-metallicity and Curie temperature of Tc-doped Janus MoSSe monolayer. Mat Chem Phys 307:128149. https://doi.org/10.1016/j.matchemphys.2023.128149

17. Nazir S (2024) DFT perception on the electronic, magnetic properties, and Curie temperature in transition elements-doped MoSeTe Janus monolayer. Mat Sci Semicond Proc 173:108135. https://doi.org/10.1016/j.mssp.2024.108135

18. Jun L, Cheng-Cai H, Yang W, Qian Y, Lian-Yan W, Deng-Feng L (2022) A promising robust intrinsic half-metallic MXene nanosheet Cr_2CuC_2 with high Curie temperature. Physica E 143:115276. https://doi.org/10.1016/j.physe.2022.115276

19. Zhou H, Tang H, Yuan H, Chen H (2022) Room-temperature half-metallicity in rich Ti-alloyed $CrSi_2N_4$ monolayer. J Mag Mag Mat 562:169742. https://doi.org/10.1016/j.jmmm.2022.169742

20. Özdemir EG, Merdan Z (2021) First-principles calculations to investigate half-metallic band gap and elastic stability of Co(Mo, Tc)MnSb compounds. Physica E 133:114790. https://doi.org/10.1016/j.physe.2021.114790

21. Rashko MN, Othman MS, Hamad AH (2022) Effects of doping cadmium atoms on the electronic and optical properties of (n,0) zigzag SWCNTs: DFT approach. ECS J Sol St Sci Tech 11:081009. https://doi.org/10.1149/2162-8777/ac861b

22. Alyami M, Alfrnwani OA, Othman MS, Elkenany EB (2024) Computational study of lattice dynamics and mechanical properties of $Al_xIn_{1-x}P_ySb_zAs_{1-y-z}$/InP under the effect of composition. Phys Scripta 99:065701. https://doi.org/10.1088/1402-4896/ad46ce

23. Azadparvar M, Rahnamaye Aliabad HA, Özdemir EG (2023) Optoelectronic and thermoelectric properties of Sb_2S_3 under hydrostatic pressure for energy conversion. AIP Adv 13:065218. https://doi.org/10.1063/5.0151650

24. Rahnamaye Aliabad HA, Arzefforni AA, Sadati SZ, Özdemir EG (2024) High-performance optoelectronic and thermoelectric properties of transparent conductors based on Tl_2O_3 under pressure. Sci Rep 14:9237. https://doi.org/10.1038/s41598-024-58657-9

25. Nazir S (2024) Insulator-to-metal transition, magnetic anisotropy, and improved TC in a ferrimagnetic La_2CoIrO_6: strain influence. Phy Chem Chem Phys 26:5002–5009. https://doi.org/10.1039/d3cp04755e

26. Algahtani A, Ali S, Hussain T, Ali A, Quraishi AM, Tirth V, Abdullaeva BS, Kamran M, Aslam M, Zaman A (2024) Studies on structural, optical and microwave dielectric properties of double perovskite $Sr_2Fe_{1+x}Nb_{1-x}O_6$, ceramics synthesized by solid state route. Opt Mat 148:114822. https://doi.org/10.1016/j.optmat.2023.114822

27. Liu X, Wu Z, Fu X, Tang L, Li J, Gong J, Xiao X (2021) Highly efficient wide-band-gap perovskite solar cells fabricated by sequential deposition method. Nano Energy 86:106114. https://doi.org/10.1016/j.nanoen.2021.106114

28. Sun T, Ma Z, Yao M, Wei J, Liu Y, Ming X (2023) Direct band-gap iodide double perovskite solar cell materials by doping strategy: First-principles predictions. Mat Today Comm 37:107055. https://doi.org/10.1016/j.mtcomm.2023.107055

29. Muddelwar RK, Pani J, Lad AB, Borkar H (2024) Gaikwad VM (2024) A novel double perovskite Dy_2CoMnO_6 as supercapacitor electrode with efficient electrochemical performance. J Sol Sta Chem 329:124455. https://doi.org/10.1016/j.jssc.2023.124455

30. Bairwa JK, Kamlesh PK, Rani U, Singh R, Gupta R, Kumari S, Kumar T, Verma AS (2024) Highly efficient and stable Ra_2LaNbO_6 double perovskite for energy conversion device applications. Mat Sci En Tech 7:61–72. https://doi.org/10.1016/j.mset.2023.07.005

31. Zanib M, Mustafa GM, Iqbal MW, Younas B, Mahmood A, Iqbal M (2024) Half metallic ferromagnetism in Ba_2XIrO_6 (X = Y, La, Sc) double perovskites for energy storage applications. Mat Sci Semicond Proc 169:107890. https://doi.org/10.1016/j.mssp.2023.107890

32 Berri S (2020) First-principles search for half-metallic ferromagnetism in double perovskite X_2MnUO_6 (X = Sr or Ba) compounds. Acta Phys Pol A 138:834–837. https://doi.org/10.12693/APhysPolA.138.834

33. Berri S (2021) Half-metallic and thermoelectric properties of Sr_2EuReO_6. Comp Cond Mat 28:e00586. https://doi.org/10.1016/j.cocom.2021.e00586

34. Berri S (2015) First-principles study on half-metallic properties of the Sr_2GdReO_6 double perovskite. J Mag Magn Mat 385:124–128. https://doi.org/10.1016/j.jmmm.2015.03.025

35. Usman M, Pan D, Kashif Masood M, Zhang C (2024) Mn-based hydride perovskites XMnH3 (X = K, Li): A DFT study for physical properties, and hydrogen storage capability. Sol St Comm 390:115600. https://doi.org/10.1016/j.ssc.2024.115600

36. Tang T, Tang Y (2024) Lithium doping in Na-based double perovskite for hydrogen storage and improving their optoelectronic properties: First-principles investigation. Mat Chem Phys 316:129099. https://doi.org/10.1016/j.matchemphys.2024.129099

37. Pakravesh F, Izadyar M (2024) Theoretical insights into the electronic and optical properties of lithium-based perovskite for solar cell applications. J Photochem Photobio A: Chem 453:115602. https://doi.org/10.1016/j.jphotochem.2024.115602

38. Blaha P, Schwarz K, Madsen GKH, Hvasnicka D, Luitz J, Schwarz K (2001) WIEN2k, an augmented plane wave plus local orbitals program for calculating crystal properties. Vienna University Technology, Vienna

39. Blaha P, Schwarz K, Tran F et al (2020) The J Chem Phys 152:074101. https://doi.org/10.1063/1.5143061

40. Perdew JP, Burke K, Ernzerhof M (1996) Generalized Gradient Approximation Made Simple. Phy Rev Lett 77:3865. https://doi.org/10.1103/PhysRevLett.77.3865

41. Perdew JP, Burke K, Wang Y (1996) Generalized gradient approximation for the exchange-correlation hole of a many-electron system. Phy Rev B 54:16533–16539

42. Bennett LJ, Jones G (2014) The influence of the Hubbard U parameter in simulating the catalytic behaviour of cerium oxide. Phys Chem Chem Phys 16:21032. https://doi.org/10.1039/c4cp00928b

43. Dar SA, Srivastava V, Sakalle UK, Rashid A, Pagare G (2018) First-principles investigation on electronic structure, magnetic, mechanical and thermodynamic properties of SrPuO3 perovskite

oxide. Mat Res Express 5:026106. https://doi.org/10.1088/2053-1591/aaabcd

44. Özdemir EG (2022) Comparisons of the magnetic and half-metallic properties of Sb-V-Te compounds in low and rich vanadium region. J Supercond Novel Magn 35:3745–3759. https://doi.org/10.1007/s10948-022-06441-z

45. Otero-de-la Roza A, Abbasi-Pérez D, Luaña V (2011) Gibbs2: A new version of the quasiharmonic model code. II. Models for solid-state thermodynamics, features and implementation. Comp Phys Commun 182:2232–2248. https://doi.org/10.1016/j.cpc.2011.05.009

46. Otero-de-la Roza A, Luaña V (2011) Gibbs2: A new version of the quasi-harmonic model code. I. Robust treatment of the static data. Comp Phys Commun 182:1708–1720. https://doi.org/10.1016/j.cpc.2011.04.016

47. Murnaghan FD (1944) The Compressibility of media under extreme pressures, proceedings of the National Academy of Sciences, United States of America 30:9. https://doi.org/10.1073/pnas.30.9.244

48. Nazir S, Akbar W, Naseem S, Zulfiqar M, Alay-e-Abbas SM, Ni JJ (2023) Emergence of robust half-metallic spin gap and a sizeable magnetic anisotropy in electron-doped Ca_2FeOsO_6. Mat Chem Phy 294:126946. https://doi.org/10.1016/j.matchemphys.2022.126946

49. Chen W, George J, Varley JB, Rignanese GM, Hautier G (2019) High-throughput computational discovery of $In_2Mn_2O_7$ as a high Curie temperature ferromagnetic semiconductor for spintronics. NPJ Comp Mat 5:72. https://doi.org/10.1038/s41524-019-0208-x

50. Petit AT, Dulong PL (1819) Recherches sur Quelques Points Importants de la Theorie de la Chaleur. Ann Chim Phys 10:395–413